NANO · MICRO small
www.small-journal.com

3D Printing Temperature Tailors Electrical and Electrochemical Properties through Changing Inner Distribution of Graphite/Polymer

*Christian Iffelsberger, Cameron W. Jellett, and Martin Pumera**

The rise of 3D printing technology, with fused deposition modeling as one of the simplest and most widely used techniques, has empowered an increasing interest for composite filaments, providing additional functionality to 3D-printed components. For future applications, like electrochemical energy storage, energy conversion, and sensing, the tuning of the electrochemical properties of the filament and its characterization is of eminent importance to improve the performance of 3D-printed devices. In this work, customized conductive graphite/poly(lactic acid) filament with a percentage of graphite filler close to the conductivity percolation limit is fabricated and 3D-printed into electrochemical devices. Detailed scanning electrochemical microscopy investigations demonstrate that 3D-printing temperature has a dramatic effect on the conductivity and electrochemical performance due to a changed conducive filler/polymer distribution. This may allow, e.g., 3D printing of active/inactive parts of the same structure from the same filament when changing the 3D printing nozzle temperature. These tailored properties can have profound influence on the application of these 3D-printed composites, which can lead to a dramatically different functionality of the final electrical, electrochemical, and energy storage device.

1. Introduction

The recent explosion in interest for additive manufacturing,[1] more specifically, fused deposition modeling (FDM),[2] direct ink writing,[3] stereo lithography,[4] and related processes, has revolutionized both rapid prototyping and the mass fabrication of custom objects for commercial, academic, and hobbyist interests alike. In FDM, a molten thermoplastic filament is extruded through a movable nozzle to form the desired part layer-by-layer. With growing interest in the FDM printing process, the number of available filament materials is constantly increasing.[2,5] The majority of polymers used for FDM are insulators like poly(lactic acid) (PLA), glycolated poly(ethylene terephthalate (PEGT), and a co-polymer of acrylonitrile, 1,3-butadiene, and styrene (ABS), and, as such, their use is purely structural.[6] The pursuit of more powerful applications requires the development of novel filaments with customized compositions for specialized functionalities (conductivity, thermoelectric properties, etc.). Because conductive and semiconductive polymers are usually not thermoplastics (there are some notable exceptions),[7,8] the most straightforward way to impart functional characteristics is by blending the polymers with functional fillers. Typically used filler materials in commercial and customized conductive FDM filaments are carbon-based materials like graphite,[9] graphene and reduced graphene oxide,[10,11] carbon black,[12]

Dr. C. Iffelsberbger, Prof. M. Pumera
Future Energy and Innovation Laboratory
Central European Institute of Technology
Brno University of Technology
Purkyňova 123, Brno 61200, Czech Republic
E-mail: martin.pumera@ceitec.vutbr.cz

Dr. C. W. Jellett, Prof. M. Pumera
Center of Advanced Functional Nanorobots
Department of Inorganic Chemistry
Faculty of Chemical Technology
University of Chemistry and Technology in Prague
Technická 5, Prague 16628, Czech Republic

The ORCID identification number(s) for the author(s) of this article can be found under https://doi.org/10.1002/smll.202101233.

DOI: 10.1002/smll.202101233

Prof. M. Pumera
Department of Chemical and Biomolecular Engineering
Yonsei University
50 Yonsei-ro, Seodaemun-gu, Seoul 03722, Korea

Prof. M. Pumera
3D Printing & Innovation Hub
Department of Chemistry and Biochemistry
Mendel University in Brno
Zemedelska 1, Brno CZ-613 00, Czech Republic

Prof. M. Pumera
Department of Medical Research
China Medical University Hospital
China Medical University
No. 91 Hsueh-Shih Road, Taichung 40402, Taiwan

and carbon nanotubes[13] in combination typically with PLA. A notable exception to this trend is from the Grayson group,[14] where composite filaments of thermoelectric bismuth telluride (both n- and p-type) were extruded using plasticizer to enable both such a high loading of the active material and the ability to extrude the composite.

3D printing of electrochemical devices[15] used for energy storage,[16] energy conversion,[17–19] or sensing applications,[20–23] usually uses carbon-based conductive filaments. The formed structures are conductive, but their electrochemical application often requires post-printing activation procedures by solvent treatment,[22,24] thermal treatment,[25,26] or hydrolysis (electrochemical[27–29] or enzymatic[30]). Simultaneously, the formed composite should retain both the processability of the inert binder polymer and the desired characteristics of the filler.

For electrical and electrochemical applications, the conductivity and electrochemical activity are crucial properties and their detailed study is of great importance. It is known that parameters like the shape[31] and composition[12] of the conductive filler influence the formation of conductive networks inside the extruded composites with carbon-based fillers. Commonly, the performance is directly examined by direct use in the intended application followed by evaluation of its macroscopic properties.[10,18,32–35] However, this provides only averaged performance information about the complete tested structure, i.e., local differences are neglected, which can lead to misinterpretations because catalytic activities can be highly localized. Electroanalytical instruments like the scanning electrochemical microscope (SECM) are powerful tools for the detailed investigation of electrochemical activity, surface morphologies, and electrochemical reactions.[36–38] The SECM allows the highly localized and destruction free in situ probing of the electrochemical activity of composite materials and 3D-printed parts by scanning an ultramicroelectrode (UME, per convention, are electrodes having at least one dimension, such as the radius of a disk or the width of a band smaller than 25 µm)[39] across the substrate.[40–42] Thus, SECM provides an ideal platform for investigating the filler/continuous phase distribution of carbon-polymer composite material as it can clearly differentiate between conductive carbon and insulating polymer at resolution of 10 µm.

Herein, we show that slight changes of 3D printing head temperature (ΔT = 25 K, ≈5%) can dramatically change the inner structure of composite and, subsequently, the electrical and electrochemical properties of the final printed piece. As we show by SECM investigations of the electrochemical activity of the 3D-printed parts and the original filament, this is due to temperature-dependent changes in the distribution of graphite filler in the nonconductive polymer continuous phase. This serves not only as a warning to exactly monitor the temperature of a 3D print but also reveals the possibility for tailoring conductive/electrochemically active and nonconductive/electrochemically inactive parts of the same device via simple changes in the 3D printing temperature.

2. Results and Discussion

Because composite filaments can, in general, extend both the applicability of FDM and the functionality for advanced electrochemical applications, we fabricated the bespoke graphite/PLA filament, and used it to 3D-print electrochemical devices by FDM. Similar to previous reports by Foster et al.,[43] we found a percolation limit between 20% and 30% mass loading of graphite because the fabricated filament with 30% mass loading showed

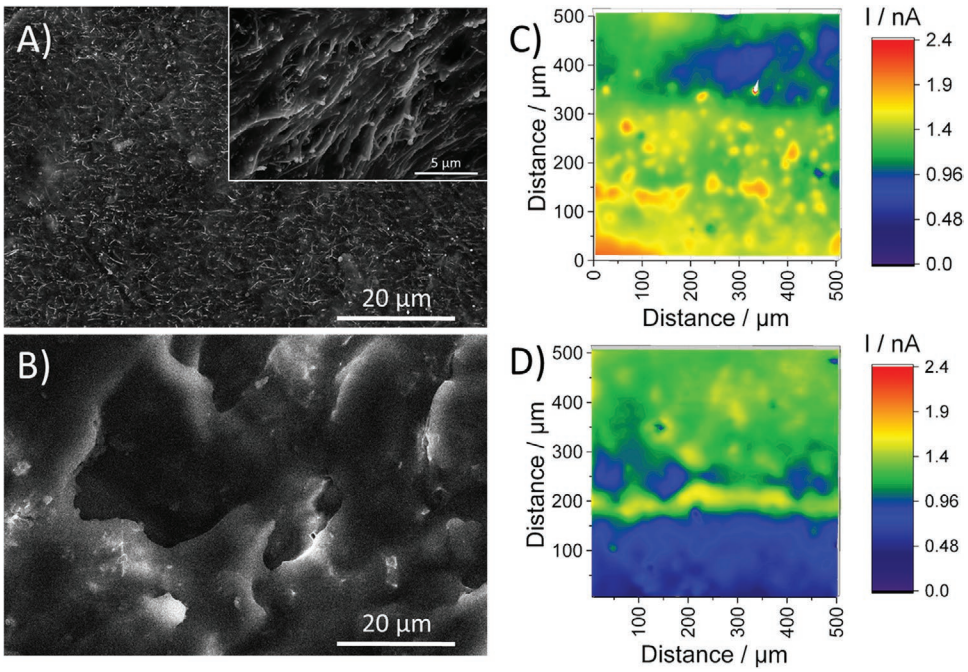

Figure 1. Scanning electron and scanning electrochemical micrographs of freshly printed A,C) nanocarbon/PLA and B,D) graphite/PLA electrodes (T_{nozzle} = 220 °C). The inset in (A) shows the nanocarbon/PLA surface with higher magnification. SECM images were recorded with a 10 µm diameter Pt disk UME at an applied potential of E_{UME} = 0.4 V, a pixel size of 6 µm, and 100 µm s^{-1} scan speed.

conductive and electrochemical activity, whereas a similar fabricated filament with 20% mass loading was effectively an insulator. Additionally, the percolation model has been shown to be a good fit for graphite/polymer composite, where the relationship between volume of conductive material and conductivity shows an S-shaped curve with a defined percolation threshold.[44,45] This indicates that the conductivity of the composed material is derived from an infinite network-type transport mechanism. For reference, a commercial nanocarbon/PLA filament was also used. We employed scanning electron microscopy (SEM) to obtain microscopic images and SECM to map conductivity and electrochemical activity with a resolution of 10 µm. SEM images of printed nanocarbon/PLA (commercial filament) and graphite/PLA (custom filament) structures are shown in **Figure 1**A,B, respectively. It is visible that the nanocarbon/PLA surface is rough, with small rod-like structures of diameters less than 1 µm and several µm in length encapsulated in the polymer matrix. Previous studies identified these structures as the carbon nanotubes,[46] with their ends facing out of the surface as visible in the inset. In comparison, the surface of the graphite/PLA electrode shows graphite particles of a few micrometer diameter enclosed by PLA. SECM imaging in feedback mode was performed for the detailed investigation of both freshly printed electrodes, where the UME is scanned parallel to the studied substrate in around one electrode radius distance. The measured signal is the electrochemical conversion of a mediator species in a diffusion-limited, reversible, one-electron reaction, depending on the conductivity of the substrate. Insulating materials like PLA and epoxy resin block the diffusion of the mediator species toward the UME, resulting in a decreased current. Conductive surfaces, like exposed conductive filler, enable the recycling of the mediator, resulting in an increased current. In summary, feedback mode provides information about the morphology and conductivity of the filler/PLA mixture. The SECM image of the nanocarbon/PLA surface (Figure 1C) shows that the surface is mostly insulating, with only confined areas in the size of few to several tenth of micrometers randomly distributed across the electrode providing conductivity (orange regions). The low activity of these areas explains the existing but low electrochemical activity of the unmodified 3D-printed electrodes. Additionally, surface roughness in the range of few µm (blue and green regions) is visible. The SECM image of the graphite/PLA electrode, Figure 1D, in contrast, shows only insulating areas and surface roughness comparable to the nanocarbon/PLA electrode. The image shows two layers of the composite material as macro-inhomogeneity caused by the 3D printing process. One layer appears as blue (0–150 µm) and the other as a green (300–500 µm) "band." The visible groove shows the intersection of these two layers. This characteristic layered structure is also visible in the upper part (350–500 µm) in Figure 1C; however, it is not as obvious in Figure 1D.

To further investigate the internal electrical and electrochemical properties of the composites, cross-sections through the filaments and corresponding 3D-printed electrodes were prepared and analyzed. Optical images of the cross-sections are shown in Figure S1A–D in the Supporting Information and display the blend of conductive filler and PLA as an optically uniform mixture. The use of graphite particles results in a reflective optical appearance. The SEM images of the examined graphite/PLA filament and electrode cross-sections (shown in Figure S1E,F, respectively, Supporting Information) clearly show inhomogeneity of the graphite and the PLA on the scale of tens of micrometers.

The characterization of the cross-sections by cyclic voltammetry showed excellent electrochemical properties as shown in Figure S2A–D in the Supporting Information. The redox peak-to-peak separations for ferrocene methanol (FcMeOH) were found to be 102 and 106 mV for the nanocarbon/PLA filament and electrode, while 127 and 120 mV for the graphite/PLA filament and electrode, respectively. Additional characterization using electrochemical impedance spectroscopy (EIS) presented in Figure S3A in the Supporting Information shows that the nanocarbon/PLA filament and 3D-printed electrode exhibit an Ohmic resistance of 13 and 14 Ω cm^2 and a charge transfer resistance of 174 and 256 Ω cm^2 when measured, respectively. For the graphite/PLA filament and the electrode 3D-printed at T_{nozzle} = 220 °C, the Ohmic resistance was measured at 70 and 119 Ω cm^2 and the charge transfer resistance was 17 and 31 k Ω cm^2, respectively. Even though the values of the graphite/PLA filament and electrode exceeded the values of the nanocarbon/PLA blend by two orders of magnitude, both composites show a higher Ohmic and charge transfer resistance after printing. A possible explanation for this observation could be the layered structure of the 3D-printed electrode, where losses at the intersection of the layers could increase losses due to incomplete fusion, resulting in increased resistance. The localized electrochemical characterization of these cross-sections via SECM is presented in **Figure 2**. In general, the feedback mode images show a clear contrast between the composite and surrounding epoxy resin matrix and the shapes correspond excellently with the optical images. In addition to the SECM-feedback mode, the substrate generation/tip collection (SG/TC) mode provides information about the electrochemical activity of the sample. In this mode, the electrochemical activity of the substrate is directly examined by the detection of a generated mediator species originating from the substrate. Different from feedback mode, where all conductive areas are visible, giving information about the exposed area of the 3D-printed electrode, the SG/TC mode provides information about electrochemically active areas. A good example for the difference of both modes is visible by comparing Figure 2E,F. While in the bottom-left corner in Figure 2E, a piece of the conductive filament is shown, it is not shown in Figure 2F; most probably, this part is disconnected from the filament. The SECM-feedback mode (Figure 2A,C,E,G) and SG/TC mode (Figure 2B,D,F,H) images were subsequently recorded and converted into histograms, cumulative histograms, and binary images, and are presented in Figure S4 in the Supporting Information, where the binary images highlight the highly active areas. In these areas, the measured currents exceeded the absolute current value measured at the UME in bulk solution via cyclic voltammetry (CV) ($|Ip|$ = 2.3 nA; a typical CV is given in Figure S7B, Supporting Information) due to the combination of the signals caused by the electrochemical conversion at the substrate and the cycling of the mediator.

For the nanocarbon/PLA filament (Figure 2A,B), the feedback mode image shows an exposed filament area of 2.56 mm^2 (which is ≈6% higher than the theoretical area derived from its diameter) with a low feedback current indicating a low

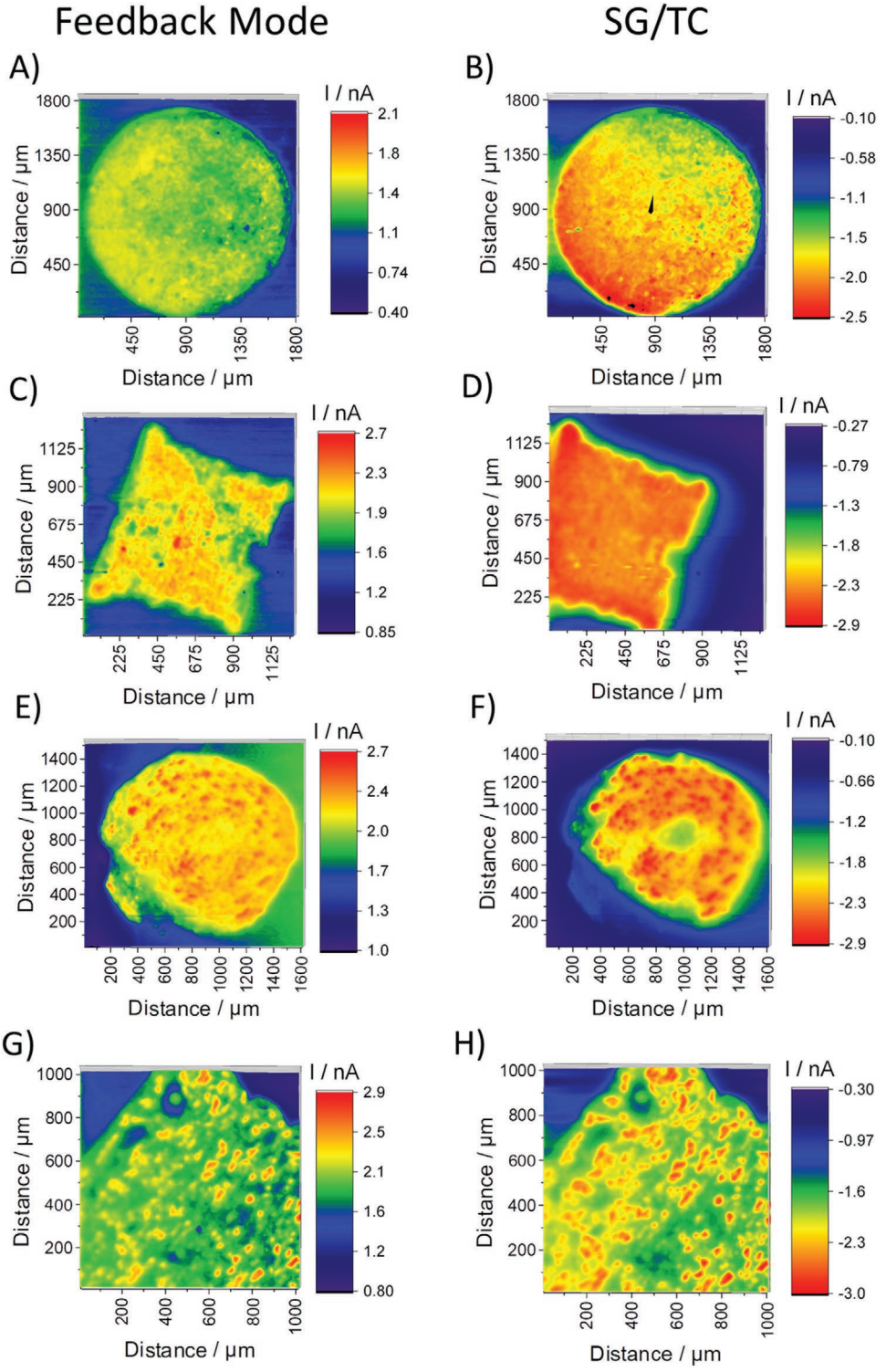

Figure 2. Scanning electrochemical characterization of cross-sections of A,B) nanocarbon/PLA filaments, C,D) corresponding 3D-printed electrode, E,F) graphite/PLA filament, and G,H) corresponding 3D-printed electrode. The applied potentials were A,C,E,G) E_{UME} = 0.4 V in feedback mode and B,D,F,H) E_{UME} = 0 V, $E_{substrate}$ = 0.6 V in SG/TC mode. Images were recorded with a 10 µm diameter Pt disk UME with 200 µm s^{-1} scan speed and a pixel size of A,B) 20 µm and C–H) 10 µm. Electrodes were 3D-printed at T_{nozzle} = 220 °C.

conductivity. In contrast, the SG/TC image shows good electrochemical activity with a few inactive spots in the size of tenths of micrometers and an electrochemically active area calculated to be ≈14% smaller (2.19 mm^2).

For the 3D-printed nanocarbon/PLA electrode recorded in feedback mode (Figure 2C), a slight distortion of the desired quadratic design with 1 mm edge length is visible, resulting in reduced exposed area of 0.81 mm^2. The appearance of the

conductivity is heterogenous with big areas of lower conductivity. The single layers from the FDM process are only slightly visible, showing good fusion of the layers during the 3D printing process. In the SG/TC image (Figure 2D), even though a minor shift of the imaged area is visible, the excellent electrochemical activity is clearly visible and the binary image shows that nearly the whole electrode area appears as one active cluster. In comparison to the commercial composite, the feedback mode image of the cross-section of the graphite/PLA filament (Figure 2E) shows a mostly conductive surface with many spots of higher conductivity (red spots) in sizes of several tenths to hundreds of micrometers. The SG/TC image (Figure 2F) shows clear differences and the electrochemical activity is clearly located at and around the conductive spots. In contrast, the corresponding graphite/PLA electrode (Figure 2G) shows high conductivity only located on very isolated spots in sizes of several tenths of micrometers. This is especially visible in the SG/TC image (Figure 2H), which shows a higher contrast and where the electrochemical activity is mostly located at the conductive areas. Higher electrochemical contrast between active spots and their surroundings compared to the filament indicates an improved dispersion of single graphite particles inside the PLA matrix. The higher temperature used for the printing (compared to the filament extrusion at 180 °C) causes a disintegration of the clusters into smaller, randomly distributed agglomerates.

The discussion presented in the previous paragraph laid the foundations for the key point of this work, which is to show that temperature of 3D printing can be used to tailor the electrical and electrochemical behavior of printed structures and create dramatically different functionalities of the final electrical, electrochemical, and energy storage device. For the investigation on the dependence of electrochemical activity with respect to the printing temperature of the graphite/PLA filament, SECM experiments were performed with cross-section samples of electrodes printed with varying nozzle temperatures (quadratic rod design, T_{nozzle} = 185, 200, and 210 °C). The corresponding CVs presented in Figure S2E–G in the Supporting Information show peak-to-peak separations of 141, 126, and 98 mV, respectively. The optical images of the cross-section samples provided in Figure S5 in the Supporting Information show good correlation with the SECM images recorded in feedback (**Figure 3**A,C,E) and SG/TC mode (Figure 3B,D,F). In general, all cross-sections show errors in the printing of the FDM layers that resulted in reduced electrode areas of 0.61, 0.84, and 0.73 mm^2 for printing at 185, 200, and 210 °C, respectively. The effective electrode areas of the 185, 200, and 210 °C samples appear as similar size with areas of 0.59, 0.79, and 0.77 mm^2, respectively. The single layers

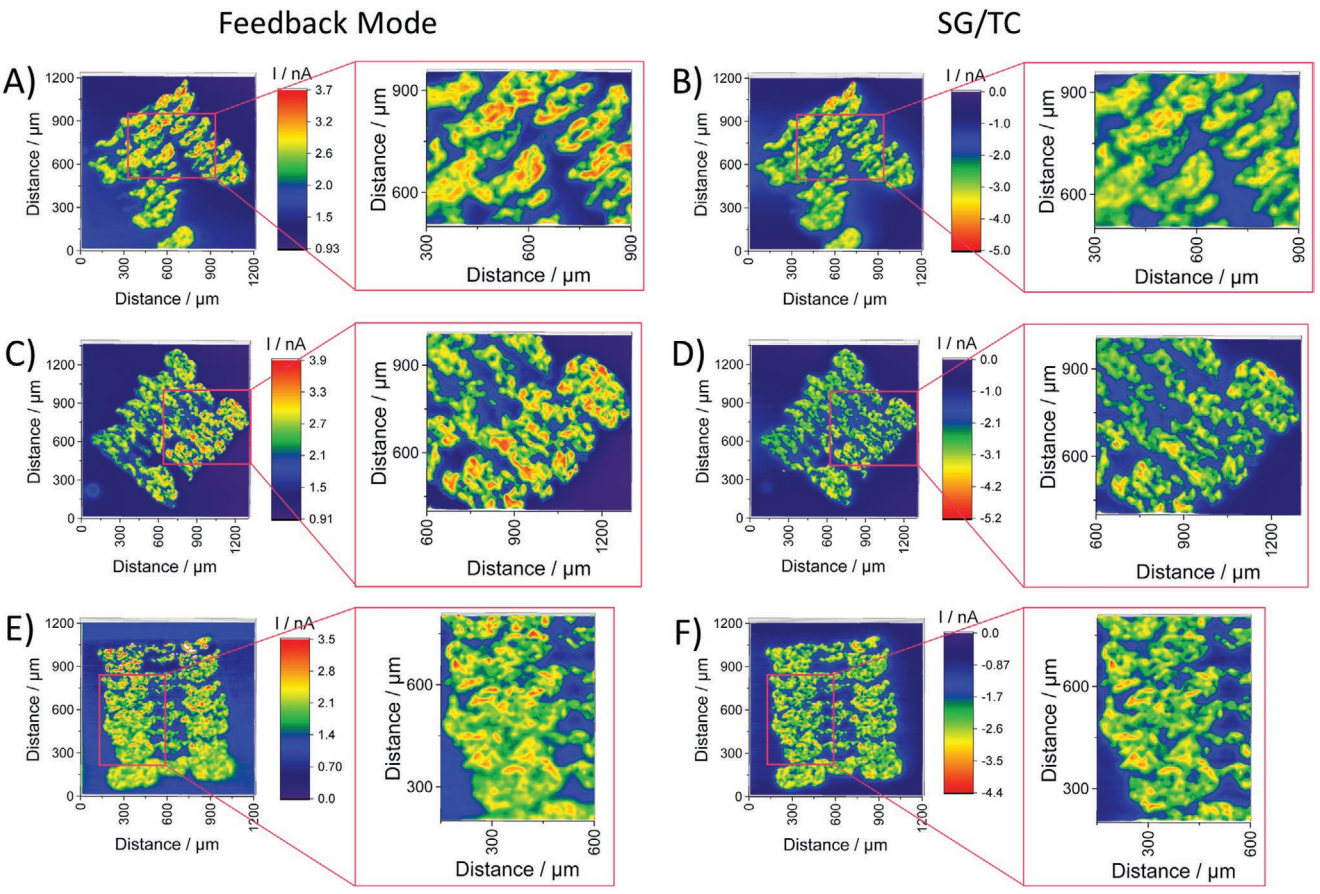

Figure 3. Scanning electrochemical characterization of cross-sections through 3D-printed graphite/PLA electrodes printed with A,B) T_{nozzle} = 185 °C, C,D) 200 °C, and E,F) 210 °C. The applied potentials were A,C,E) E_{UME} = 0.4 V in feedback mode and B,D,F) E_{UME} = 0 V, $E_{substrate}$ = 0.4 V in SG/TC mode. Images were recorded with a 10 µm diameter Pt disk UME with 100 µm s^{-1} scan speed and pixel size of 10 µm.

produced by the FDM process are clearly resolved and the fusion of the layers is poor in each case. Despite this, all cross-sections exhibit conductivity and electrochemical activity. The increasing dispersion of the graphite particles inside the PLA matrix with increasing nozzle temperature is shown in the first instance by the decrease of electrochemically highly active areas and expressed as a percentage of the effective electrode area. It was found that the highly active areas for the filament and electrode printed at T_{nozzle} = 185 °C were 63% and 66%, respectively. 3D printing at higher temperatures reduced this portion to 44% and 16% for the electrodes printed at T_{nozzle} = 210 °C and T_{nozzle} = 220 °C, respectively. Furthermore, analysis of the binary images presented in Figure S6C,F,I,L in the Supporting Information shows that with higher printing temperatures, the number of the highly active clusters increases from eight at T_{nozzle} = 185 °C to 110 at T_{nozzle} = 210 °C. This is also reflected by the sizes of the clusters with the highest surface area and average surface area per cluster. While the biggest cluster in the print with T_{nozzle} = 185 °C contributes 47% to the highly active surface area, the respective cluster in the print with T_{nozzle} = 220 °C contributes only 8%. For detailed information, a summary of the results is provided in Table S1 in the Supporting Information. The EIS measurements given in Figure S3B in the Supporting Information show that for the electrodes printed with T_{nozzle} = 185, 200, and 210 °C, an Ohmic resistance of 54, 30, and 31 Ω cm^2 and a charge transfer resistance of 436, 395, and 253 Ω cm^2 was measured, respectively. This indicates a trend of decreased Ohmic and charge transfer resistance with increasing printing temperature. The results obtained with SECM show that for the graphite/PLA composite, a higher printing temperature results in more heterogenous activity as represented by more numerous and isolated clusters. These observations correspond to the theoretical calculations of Dhillon and Kant for heterogenous electrodes with distributed charge transfer resistance.[47] They predicted that a heterogenous electrode shows a faster charge transfer due to the presence of reactive sites where the charge transfer occurs dominantly. Experimentally, for graphite composited electrodes, such behavior could be observed in the work by Li et al.[48] In their study, the heterogeneity of the electrode was created by blending graphite with graphite oxide and in EIS experiments the blend showed decreased charge transfer resistance for the composite electrode compared to the pure graphite electrode. This shows that during 3D printing, the nozzle temperature strongly influences the dispersion of the graphite particles. The lowered viscosity caused by the higher printing temperature (compared to the filament extrusion at 180 °C) could possibly enable an enhanced dispersion of the graphite particles by increasing the wetting with the polymer matrix, resulting in fewer connections between the graphite particles.[44] As a consequence, bigger conductive clusters disintegrate into smaller, randomly distributed agglomerates. This increases the heterogeneity of the composite as shown by EIS measurements and the percolation concentration. In summary, all measurements show clear influence of the printing temperature on the electrochemical properties, confirming that the electrochemical properties of 3D-printed devices can be tailored with the printing temperature.

Because nanocarbon/PLA electrodes often show low electrochemical performance directly after printing, different chemical and physical procedures for their activation have been developed. Especially, thermal activation in air is assumed to result in a nearly complete removal of the PLA by its pyrolysis into water and CO_2, leaving behind a porous 3D carbon nanostructure in its initial 3D-printed shape.[18] These structures offer a high surface area to volume ratio and have been already successfully applied as current collectors for the hydrogen evolution reaction.[18,49] In **Figure 4**A, an optical image and scanning electrochemical characterization (Figure 4B,C) of cross-sections of a thermally activated 3D nanocarbon electrode are shown. The dimensions of the freshly printed electrode before the activation procedure were equal to the electrode shown in Figure 3G. After the thermal activation procedure, the shape remained, though the encapsulation in epoxy resin caused a swelling of the nanocarbon structure from ≈1 mm^2 exposed cross-section surface of the freshly printed electrode to ≈2 mm^2 of the thermally activated electrode. This shows that by a simple thermal activation at only 350 °C in air, a predesigned 3D-printed carbon nanotube network can be formed as shown in literature.[26,46] However, the CV of the prepared cross-section shows a peak-to-peak separation of 142 mV (Figure S2H, Supporting Information). The SECM images recorded in feedback mode (Figure 4B) and SG/TC mode (Figure 4C) show a good match and a mostly electrochemically active surface as shown by the histograms in Figure S8 in the Supporting Information. The visible shift of currents shows an initially reduced feedback current of the surface in feedback mode; filling of the porous structure with epoxy resin resulted in confined areas without

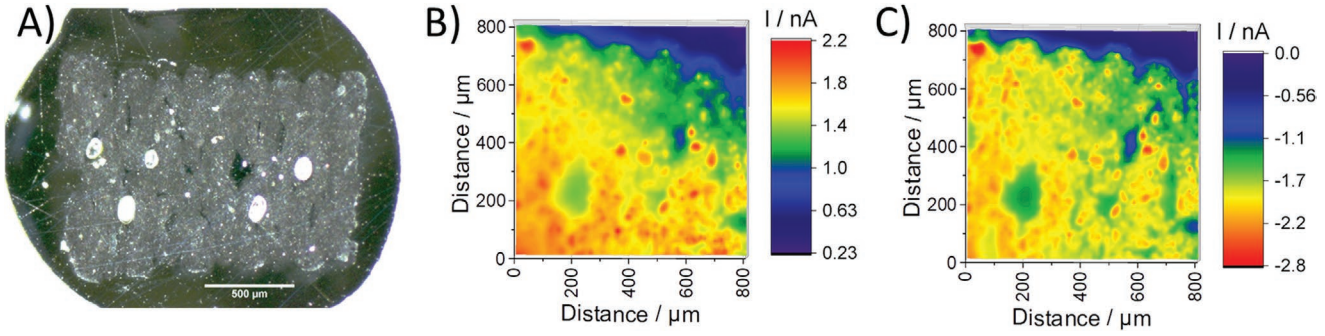

Figure 4. A) Optical image and B,C) scanning electrochemical micrographs of a cross-section through a thermally activated nanocarbon/PLA electrode. The applied potentials were B) E_{UME} = 0.4 V in feedback mode and C) E_{UME} = 0 V, $E_{substrate}$ = 0.6 V in SG/TC mode. Images were recorded with a 10 µm diameter Pt disk UME with 200 µm s^{-1} scan speed and pixel size of 10 µm.

nanocarbon, which are easily identified by SECM. In general, the results show the broad applicability of the SECM for the detailed study of 3D-shaped structures and networks.

3. Conclusion

In this study, a customized graphite/PLA filament for FDM was fabricated and used to print electrodes and compared with a commercial conductive nanocarbon-based filament. SECM is used as the main tool to investigate the electrochemical activity of a cross-section through the initial filament and 3D-printed electrochemical devices. It was found that 3D printing at higher nozzle temperatures (T_{nozzle} > 200 °C) enhances the dispersion of graphite particles in the PLA matrix, which leads to a detrimental effect on the electrochemical performance depending on the extrusion temperature. Comparison with a commercial filament as well as the study of thermally activated nanocarbon/PLA electrodes indicates the general applicability of SECM for the localized electrochemical characterization of conductive filaments, 3D-printed electrochemical devices, and conductive structures. These findings have a profound impact on the 3D printing of carbon/polymer composites as the functionality of the resulting structures is dramatically influenced by the distribution of carbon filler particles and, therefore, by the 3D printing nozzle temperature. This could be utilized to controllably 3D-print fully functional devices comprising electrochemically active/inactive parts fabricated from the same filament by varying only the printing temperature. In general, this article also provides a warning that even very small (in single % digits) variations of the 3D printing temperature can lead to dramatically different functionalities in the final electrical, electrochemical, and energy storage device.

4. Experimental Section

Chemicals: The SECM mediator solution was consisted of 1.5×10^{-3} M (FcMeOH, 99%, ABCR, Germany) with 0.2 M KNO_3 (analytical grade, Merck KGaA, Germany) as supporting electrolyte. The solution was prepared in deionized water with a resistivity of 18 MΩ cm. Dichloromethane was sourced from Penta (Czech Republic), and PLA (Ingeo2003D natural) from NatureWorks (USA). Graphite powder (<20 µm, synthetic) and PEG-750 (poly(ethylene glycol) monomethyl ether, Mn 750 Da) were purchased from Sigma-Aldrich and used without further purification.

Instrumentation: A Prusa i3 MK3 printer (Prusa Research, Czech Republic) was used to 3D print the electrodes. The nozzle diameter was 0.4 mm unless stated otherwise. Slicing of the designed electrode was done in Slic3r Prusa software (Prusa Research, Czech Republic). All electrochemical measurements were performed using an Autolab Bipotentiostat/Galvanostat (Metrohm, Netherlands) equipped with an SECM (Sensolytics, Germany) operated with the provided software. Imaging was done with a commercial Pt disk UME with 10 µm diameter and a tip-to-electrode ratio of RG > 10 (Sensolytics, Germany). Nova 2.1 software was used for CV and data processing was performed with Gwyddion 2.55 and OriginPro 2019 software. All measurements were performed using an Ag/AgCl 3 M KCl reference electrode and all reported potentials referred this electrode. Optical images of the cross-section samples were obtained using a stereomicroscope (Stemi 508, Zeiss, Germany) with color camera (Axiocam 105, Zeiss, Germany) connected to Axio Vision Software. Scanning electron microscopy was performed with Verios 460 L (FEI).

Fabrication of Graphite Filament: Because composite filaments could, in general, extend both the applicability of FDM and the functionality of the printed parts, the interest to produce customized filaments in economical scale (≈100 g) for advanced electrochemical applications was present. Fabrication of the graphite/PLA filament is presented in **Figure 5**. For the casting of a thin and flexible graphite/PLA film with all other additives already present, PLA pellets (30 g) were dissolved in 300 mL of dichloromethane with stirring, to which PEG-750 (7 g) and then graphite powder (30 g) was added. This mixture was bath-sonicated for 15 min and then poured into an evaporation dish (16 h) to

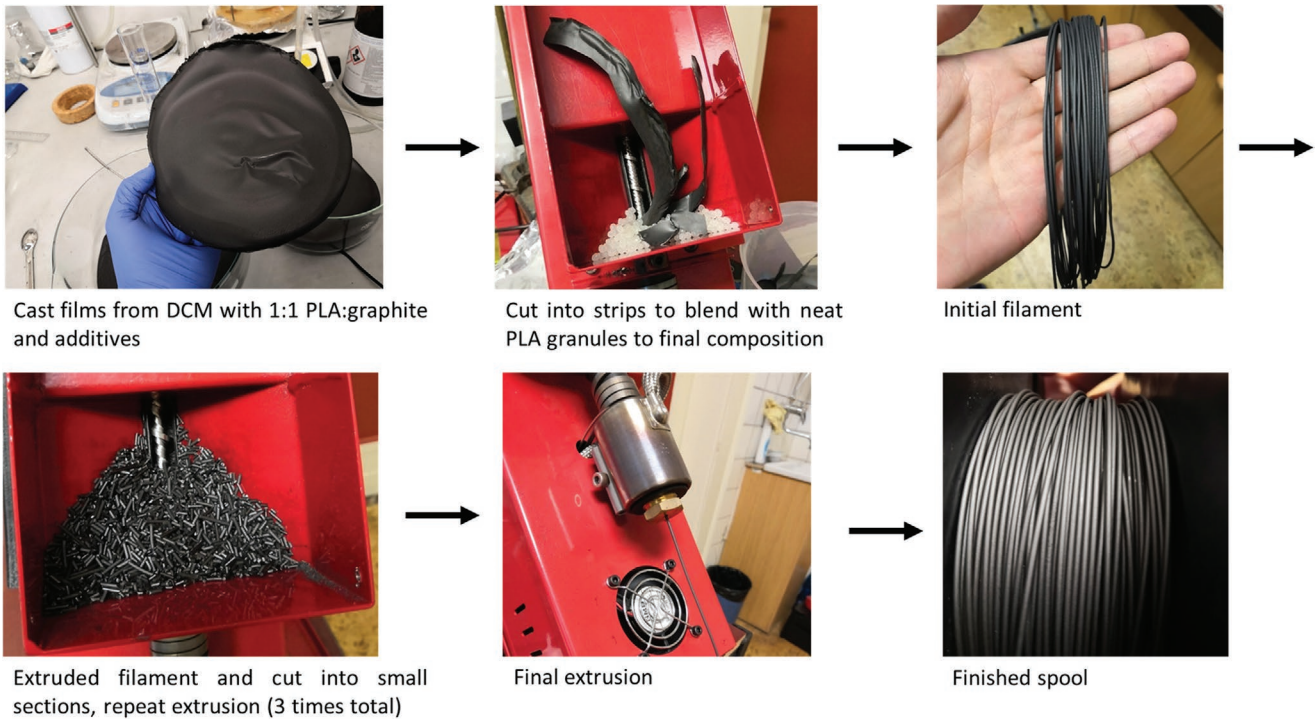

Figure 5. Workflow of the filament fabrication.

form a thick film. The film was placed in a vacuum oven (3 mbar, 40 °C) for 2 h to ensure complete solvent removal. This film was then cut into strips and fed into a Noztek Pro extruder (extrusion temperature: 180 °C) and further blending with PLA was done to bring the total mass of the composite to 100 g. It was important to monitor the mixing process constantly so as not to shear the screw shaft. The extruder was previously primed with neat PLA. For the composite mixing, the first section of the filament was discarded until a visually homogenous color was observed. Once all of the material was passed through the extruder, the filament was cut into 2–4 mm pieces and, for further homogenization of all components, re-extruded in an identical manner. This was repeated three times in total. The final extrusion was carried out at a lower temperature (168–172 °C) to maximize the thickness of the final product, and was then rolled directly onto a spool. The fabricated filaments had a diameter of 1.5 mm and a 2-point probe conductivity of 6 kΩ cm^{-1} and electrochemical activity. This was in agreement to previous reports for 30% mass loading of graphite. In general, the filament was flexible enough to bend and hard enough to be fed into the FDM printing head.

Printing of Electrodes: 3D printing of electrodes with conductive nanocarbon/PLA filament (3DBlackMagic, Graphene Lab Inc., USA) was done at T_{nozzle} = 220 °C nozzle and 60 °C bed temperature. The nanocarbon/PLA electrodes served as reference. Graphite/PLA electrodes were printed at T_{nozzle} = 185, 200, 210, and 220 °C nozzle and 60 °C bed temperature, whereas for the printing at T_{nozzle} = 220 °C, a nozzle diameter of 0.6 mm was used. Optical images of the graphite/PLA electrodes printed with different nozzle temperatures (Figure S9, Supporting Information) showed that 3D printing at 185 °C was possible, albeit the quality was poor and the adhesion between single lines was very weak. The best printing result was achieved with 220 °C. For simpler SECM analysis, a design consisting of a quadratic rod of 1 mm edge length and 3 cm length was used. For the investigation of the internal conductive network, cross-section samples of the filaments and 3D-printed electrodes were prepared. Recently, nanocarbon/PLA electrodes were thermally activated by removing the PLA to reveal the nanocarbon network.[18] For the SECM of such a network, thermal activation of the nanocarbon/PLA composite was done with the quadratic rod design in a furnace (Elektrické pece Svoboda, Czech Republic) at 350 °C for 3 h in air at ambient pressure. The heating rate was 5 °C min^{-1} starting from room temperature. Afterward, the activated electrodes were cooled down naturally to room temperature.

Preparation of Cross-Sections: First, the 3D-printed electrodes were encapsulated in two-component epoxy resin following company procedures (12.5 g of EpoFix Resin and 1.5 g of EpoFix Hardener, Struers Aps, Denmark) using a plastic holder and vacuum impregnation chamber (CITOVAC, Struers Aps, Denmark). Curing of the resin took place overnight at room temperature. Afterward, mechanical grinding and polishing were performed using a grinder/polishing machine (TEGRAMIN 30, Struers Aps, Denmark). Both sides of the encapsulated sample were ground using a MD Gekko adapter and a series of SiC grinding foils (180, 500, 1200, and 4000 grit size). Mirror-like polishing was only done on the side used for SECM examination with the diamond suspension polishing fluids (DP-Suspension P with 9, 3, and 1 µm) on an MD Nap-T polishing cloth. For utilization of the cross-section sample as an electrode, the other side was fixed with silver conductive epoxy adhesive (8330, MG Chemicals, Canada) on a copper tape supported with a glass slide in order to ensure very good and uniform electrical contact. Optical images of a cross-section sample are provided in Figure S10 in the Supporting Information.

Electrochemical Characterizations of the 3D-Printed Electrodes: The electrochemical performance of the 3D-printed electrodes was characterized by CV and SECM experiments, both in FcMeOH mediator solution. In CV measurements, the potential was cycled between $E_{vertex1}$ = −0.5 V and $E_{vertex2}$ = 1 V with a scan rate of 20 mV s^{-1}. EIS measurements were performed in FcMeOH mediator solution with a potential of E = 0.2 V (vs Ag/AgCl 3 M KCl) applied to the composites. The frequency ranged from 0.1 MHz to 0.1 Hz, with 10 mV amplitude. In SECM measurements, the UME was electrochemically characterized via CV after polishing (0.05 µm Al_2O_3 particles). The potential was scanned between $E_{vertex1}$ = 0 V and $E_{vertex2}$ = 0.5 V with a scan rate of 50 mV s^{-1}. Optical images of the UME and a typical CV are provided in Figure S7 in the Supporting Information. After initial characterization, the UME was approached at an imaging distance above the epoxy resin in negative feedback.[36] For SECM imaging of the electrode surface, 3D-printed electrodes (nanocarbon/PLA and graphite/PLA) were fixed on a glass slide using two-component epoxy resin (Roxalid, Hornbach Baumarkt AG, Germany) and examined in SECM-feedback mode with E_{UME} = 0.4 V. The SECM micrographs of the cross-sections were recorded. First, feedback mode (E_{UME} = 0.4 V) images were recorded in three-electrode configuration with Pt as counter electrode and an Ag/AgCl reference electrode. Second, SG/TC mode images were recorded in a four-electrode setup with the substrate polarized at $E_{substrate}$ = 0.6 V and the UME at E_{UME} = 0 V. SECM imaging was done with a waiting time of 4 ms. Electrode areas were calculated from histograms of the SECM images recorded in feedback mode and effective electrode areas were calculated from the corresponding SG/TC mode images.

Quantification of SECM Images: Quantification of the electrode area and highly active electrode area with SECM was based on pixel counting of the recorded images. The threshold values for the exposed area and the highly active area of the 3D-printed electrode were defined according to the cumulative histograms following the principles of the feedback mode and SG/TC of the SECM.[36] In general, for the calculation of the exposed electrode area, currents exceeding the values for negative feedback measured above the epoxy resin (surrounding the 3D-printed electrode) were counted. The threshold values used for the calculation of the exposed area and electrochemically active area are given in the captions of the cumulative histograms in the Supporting Information (Figures S4 and S6, Supporting Information) of the corresponding SECM image. Additionally, to improve visualization, SECM images recorded in SG/TC mode were converted into binary black and white images as shown in Figures S4C,F,I,L and S6C,F,I in the Supporting Information. The binary images were generated using Origin 2020 data analysis software (OriginLab, USA) with the thresholds, as described above, highlighting only the highly active areas in black. Further image analysis was done by using open-source image processing software ImageJ (NIH, USA). The "Analyze Particles" function was used to count and analyze only black areas. All particles of the size 0.01-infinity $pixel^2$ were included. No edge correction and hole filling were applied. The white area was not counted. The contribution of the biggest cluster was calculated by the pixel count of the individual biggest cluster divided by the sum of pixels from all clusters and the average cluster size was used as calculated by the software.

Supporting Information

Supporting Information is available from the Wiley Online Library or from the author.

Acknowledgements

This work was supported by the project Advanced Functional Nanorobots (reg. No. CZ.02.1.01/0.0/0.0/15_003/0000444 financed by the EFRR). C.I. acknowledges the financial support by the European Union's Horizon 2020 research and innovation programm under the Marie Skłodowska-Curie grant agreement No. 888797. M.P. thanks to Ministry of Education, Youth and Sports (Czech Republic) grant LL2002 under ERC CZ program. C.I gratefully acknowledges the CzechNanoLab project LM2018110 funded by MEYS CR for the financial support of the measurements/sample fabrication at CEITEC Nano Research Infrastructure. The authors thank Dr. Gao, Dr. Ghosh and Dr. Novotný for the scientific discussion.

Conflict of Interest

The authors declare no conflict of interest.

Author Contributions

M.P. originated the project idea and supervised the work. C.J. fabricated the graphite filament. C.I. and C.J. performed 3D printing. C.I. prepared the samples and performed and analyzed the electrochemical experiments. The manuscript was written through contributions of all authors. All authors have given approval to the final version of the manuscript.

Data Availability Statement

Research data are not shared.

Keywords

3D print filament, composite, fused deposition modeling, scanning electrochemical microscopy, substrate generation/tip collection mode

Received: March 1, 2021
Revised: March 24, 2021
Published online: May 2, 2021

[1] A. J. Capel, R. P. Rimington, M. P. Lewis, S. D. R. Christie, *Nat. Rev. Chem.* **2018**, *2*, 422.
[2] N. Mohan, P. Senthil, S. Vinodh, N. Jayanth, *Virtual Phys. Prototyping* **2017**, *12*, 47.
[3] L. Li, Q. Lin, M. Tang, A. J. E. Duncan, C. Ke, *Chem. – Eur. J.* **2019**, *25*, 10768.
[4] C. Schmidleithner, D. M. Kalaskar, in *3D Printing*, Vol. *395* (Ed: D. Cvetković), IntechOpen, London **2018**, pp. 116–124.
[5] H. H. Hamzah, S. A. Shafiee, A. Abdalla, B. A. Patel, *Electrochem. Commun.* **2018**, *96*, 27.
[6] T. D. Ngo, A. Kashani, G. Imbalzano, K. T. Q. Nguyen, D. Hui, *Composites, Part B* **2018**, *143*, 172.
[7] A. Gumyusenge, D. T. Tran, X. Luo, G. M. Pitch, Y. Zhao, K. A. Jenkins, T. J. Dunn, A. L. Ayzner, B. M. Savoie, J. Mei, *Science* **2018**, *362*, 1131.
[8] A. Gumyusenge, X. Zhao, Y. Zhao, J. Mei, *ACS Appl. Mater. Interfaces* **2018**, *10*, 4904.
[9] A. Maurel, M. Courty, B. Fleutot, H. Tortajada, K. Prashantha, M. Armand, S. Grugeon, S. Panier, L. Dupont, *Chem. Mater.* **2018**, *30*, 7484.
[10] C. W. Foster, M. P. Down, Y. Zhang, X. Ji, S. J. Rowley-Neale, G. C. Smith, P. J. Kelly, C. E. Banks, *Sci. Rep.* **2017**, *7*, 42233.
[11] X. Wei, D. Li, W. Jiang, Z. Gu, X. Wang, Z. Zhang, Z. Sun, *Sci. Rep.* **2015**, *5*, 11181.
[12] H. Liu, D. Bai, H. Bai, Q. Zhang, Q. Fu, *J. Phys. Chem. C* **2018**, *122*, 4232.
[13] K. Gnanasekaran, T. Heijmans, S. van Bennekom, H. Woldhuis, S. Wijnia, G. de With, H. Friedrich, *Appl. Mater. Today* **2017**, *9*, 21.
[14] J. Peng, I. Witting, N. Geisendorfer, M. Wang, M. Chang, A. Jakus, C. Kenel, X. Yan, R. Shah, G. J. Snyder, M. Grayson, *Nat. Commun.* **2019**, *10*, 5590.
[15] A. Ambrosi, M. Pumera, *Chem. Soc. Rev.* **2016**, *45*, 2740.
[16] a) M. P. Browne, E. Redondo, M. Pumera, *Chem. Rev.* **2020**, *120*, 2783. b) J. Munoz, M. Pumera, *TrAC, Trends Anal. Chem.* **2020**, *128*, 115933.
[17] C.-Y. Lee, A. C. Taylor, A. Nattestad, S. Beirne, G. G. Wallace, *Joule* **2019**, *3*, 1835.
[18] J. P. Hughes, P. L. Dos Santos, M. P. Down, C. W. Foster, J. A. Bonacin, E. M. Keefe, S. J. Rowley-Neale, C. E. Banks, *Sustainable Energy Fuels* **2019**, *4*, 302.
[19] M. P. Browne, V. Urbanova, J. Plutnar, F. Novotný, M. Pumera, *J. Mater. Chem. A* **2020**, *8*, 1120.
[20] C. Tan, M. Z. M. Nasir, A. Ambrosi, M. Pumera, *Anal. Chem.* **2017**, *89*, 8995.
[21] E. M. Richter, D. P. Rocha, R. M. Cardoso, E. M. Keefe, C. W. Foster, R. A. A. Munoz, C. E. Banks, *Anal. Chem.* **2019**, *91*, 12844.
[22] C. L. Manzanares Palenzuela, F. Novotný, P. Krupička, Z. Sofer, M. Pumera, *Anal. Chem.* **2018**, *90*, 5753.
[23] R. M. Cardoso, C. Kalinke, R. G. Rocha, P. L. dos Santos, D. P. Rocha, P. R. Oliveira, B. C. Janegitz, J. A. Bonacin, E. M. Richter, R. A. A. Munoz, *Anal. Chim. Acta* **2020**, *1118*, 73.
[24] C. Kalinke, N. V. Neumsteir, G. D. O. Aparecido, T. V. de B. Ferraz, P. L. dos Santos, B. C. Janegitz, J. A. Bonacin, *Analyst* **2020**, *145*, 1207.
[25] F. Novotný, V. Urbanová, J. Plutnar, M. Pumera, *ACS Appl. Mater. Interfaces* **2019**, *11*, 35371.
[26] C. Iffelsberger, S. Ng, M. Pumera, *Appl. Mater. Today* **2020**, *20*, 100654.
[27] P. R. de Oliveira, C. Kalinke, J. L. Gogola, A. S. Mangrich, L. H. M. Junior, M. F. Bergamini, *J. Electroanal. Chem.* **2017**, *799*, 602.
[28] M. P. Browne, F. Novotný, Z. Sofer, M. Pumera, *ACS Appl. Mater. Interfaces* **2018**, *10*, 40294.
[29] D. M. Wirth, M. J. Sheaff, J. V. Waldman, M. P. Symcox, H. D. Whitehead, J. D. Sharp, J. R. Doerfler, A. A. Lamar, G. Leblanc, *Anal. Chem.* **2019**, *91*, 5553.
[30] a) C. L. Manzanares-Palenzuela, S. Hermanova, Z. Sofer, M. Pumera, *Nanoscale* **2019**, *11*, 12124. b) A. M. López Marzo, C. C. Mayorga-Martinez, M. Pumera, *Biosens. Bioelectron.* **2020**, *151*, 111980.
[31] A. Göldel, A. Marmur, G. R. Kasaliwal, P. Pötschke, G. Heinrich, *Macromolecules* **2011**, *44*, 6094.
[32] A. Ambrosi, M. Pumera, *Adv. Funct. Mater.* **2018**, *28*, 1700655.
[33] R. Gusmão, M. P. Browne, Z. Sofer, M. Pumera, *Electrochem. Commun.* **2019**, *102*, 83.
[34] N. Rohaizad, C. C. Mayorga-Martinez, F. Novotný, R. D. Webster, M. Pumera, *Electrochem. Commun.* **2019**, *103*, 104.
[35] M. P. Browne, M. Pumera, *Chem. Commun.* **2019**, *55*, 8374.
[36] A. J. Bard, M. V. Mirkin, *Scanning Electrochemical Microscopy*, 2nd ed., CRC Press, Boca Raton, FL **2012**.
[37] D. Polcari, P. Dauphin-Ducharme, J. Mauzeroll, *Chem. Rev.* **2016**, *116*, 13234.
[38] J. Izquierdo, P. Knittel, C. Kranz, *Anal. Bioanal. Chem.* **2018**, *410*, 307.
[39] A. J. Bard, G. Inzelt, F. Scholz, in *Electrochemical Dictionary* (Eds: A. J. Bard, G. Inzelt, F. Scholz), Springer Berlin Heidelberg, Berlin, Heidelberg **2012**.
[40] Z. Meiszterics, A. Asserghine, A. Kiss, L. Nagy, T. Zsebe, G. Nagy, *Electroanalysis* **2020**, *32*, 820.
[41] S. Viehbeck, C. Iffelsberger, F.-M. Matysik, *Composites, Part A* **2018**, *113*, 32.
[42] S. Ramírez-García, S. Alegret, F. Céspedes, R. J. Forster, *Analyst* **2002**, *127*, 1512.
[43] C. W. Foster, H. M. Elbardisy, M. P. Down, E. M. Keefe, G. C. Smith, C. E. Banks, *Chem. Eng. J.* **2020**, *381*, 122343.
[44] M. Blaszkiewicz, D. S. Mclachlan, R. E. Newnham, *Polym. Eng. Sci.* **1992**, *32*, 421.
[45] M. L. Clingerman, J. A. King, K. H. Schulz, J. D. Meyers, *J. Appl. Polym. Sci.* **2002**, *83*, 1341.
[46] S. Ng, C. Iffelsberger, J. Michalička, M. Pumera, *ACS Nano* **2021**, *15*, 686.
[47] S. Dhillon, R. Kant, *J. Chem. Sci.* **2017**, *129*, 1277.
[48] W. Li, J. Liu, C. Yan, *Electrochim. Acta* **2011**, *56*, 5290.
[49] S. Ng, C. Iffelsberger, Z. Sofer, M. Pumera, *Adv. Funct. Mater.* **2020**, *30*, 1910193.